Path Following Control of Underactuated Surface Vessels in the Presence of Multiple Disturbances

Walter Caharija, Asgeir J. Sørensen, Kristin Y. Pettersen, Marilena Greco and Jan T. Gravdahl

***Abstract*— An integral version of the line-of-sight guidance method is shown to compensate for both kinematic and dynamic disturbances generated by wind, waves and sea currents. The guidance law is designed for path following tasks of underactuated marine vessels moving in the horizontal plane. Specifically, the control system consists of an integral line-of-sight heading reference generator in a cascaded configuration with an adaptive surge-yaw controller. The total drifting effect of the environmental disturbances is modeled as a combination of a constant and unknown kinematic drift, and a constant, unknown and heading-dependent dynamic pressure acting on the vessel. The closed loop stability analysis shows that path following is achieved with global κ-exponential stability properties. The theoretical results are supported by simulations.**

I. Introduction

Control methods for path following and trajectory tracking are fundamental for autonomous ships since they make the vessel follow a predetermined path. In particular, robust path following and trajectory tracking control systems specifically designed for underactuated vessels are required to successfully enable autonomous ships since they operate in presence of disturbances such as wind, waves and ocean currents that may seriously influence the success of a mission. Such disturbances have an even greater effect when acting in the transverse abeam direction since all ships are generally underactuated at transit speed, i.e., they have no thrusters providing side force to counteract for transverse disturbances or, if they have any, they are ineffective at surge speeds higher than 2-3 knots [1]. Consequently, several robust path following and trajectory tracking solutions based on linear and nonlinear control theory have been proposed [2]–[8] and among them the integral line-of-sight (ILOS) guidance law for path following purposes ranks among the most popular ones thanks to its simplicity and intuitiveness [9]–[13].

This paper shows that the ILOS guidance law first presented in [9] successfully compensates for combined kinematic and dynamic disturbances, thus further extending the results of [10], [14]. To this end and motivated by [15], the 3 degrees-of-freedom (DOFs) maneuvering model presented in [16] is modified to include both the kinematic and dynamic disturbance effects of currents, wind and waves for control design purposes. The model separates the disturbances into an unknown irrotational current (kinematic drift/bias) and an environmental load vector (dynamic bias). Such a distinction is proposed to capture the different effects of the otherwise combined disturbances [17]. The kinematic bias account for currents, tidal drifts, low frequency swells and second order wave-induced forces, while the environmental load vector embodies the heading dependent dynamic effects of the disturbances. In this context the mean wind forces are assumed to dominate in the load vector and are modeled as an unknown pressure acting in a certain direction. The two disturbances generally act in different directions and are assumed slowly varying or here constant. The first order wave-induced forces are neglected since they cause zero mean oscillatory motions that are usually removed through wave filtering. The effect of wind gusts is either directly compensated by wind feedforward control action or by the feedback controllers. The ILOS guidance method developed in [9], [10] is extended with adaptation, and it is analytically shown that the resulting control scheme successfully compensates for both kinds of disturbances and hence guarantees path following of underactuated surface vessels in different sea conditions. Path following of straight lines is considered and, due to the integral action, the underactuated vessel is made to crab in order to compensate for the drift and follow the desired course since no actuation is available in sway. The control approach is based on relative velocities only. The combined effect of kinematic and dynamic disturbances is analyzed assuming that the dynamic disturbance is known in direction but unknown in magnitude. The mathematical analysis of the complete kinematic-dynamic closed loop system combines the results from [10] with elements of robust control of mechanical systems [18]. This shows that the ILOS guidance in a cascaded configuration with an adaptive speed-heading controller guarantees uniform global asymptotic stability (UGAS) and uniform local exponential stability (ULES) (i.e. global κ-exponential stability). Simulations are presented to verify and illustrate the theoretical results.

The paper is organized as follows: Section II presents the vessel model for control design purposes, Section III defines the control problem, while Section IV presents the ILOS guidance. Section V presents the adaptive surge-yaw controller, and the stability properties of the closed loop system are given in Section VI. The mathematical analysis is

Supported by the Research Council of Norway through the Centers of Excellence funding scheme, project number 223254 and the Strategic University Program, project number 192427.

W. Caharija is with the Center for Autonomous Marine Operations and Systems at the Norwegian University of Science and Technology and SINTEF Ocean AS, both located in Trondheim, Norway. walter.caharija@sintef.no

A. J. Sørensen, K. Y. Pettersen and M. Greco are with the Center for Autonomous Marine Operations and Systems, Norwegian University of Science and Technology, Trondheim, Norway. {asgeir.sorensen, kristin.y.pettersen, marilena.greco}@ntnu.no

J. T. Gravdahl is with the Department of Engineering Cybernetics, Norwegian University of Science and Technology, Trondheim, Norway. jan.tommy.gravdahl@ntnu.no

developed in Section VII and the simulation results are given in Section VIII. Finally, conclusions are found in Section IX.

II. The Control Plant Model

The control plant model is a simplified mathematical description of the surface vessel. It contains the physical properties that are significant for control design purposes [1].

A. Vessel Assumptions

Assumption 1. The motion of the vessel can be described by 3 degrees of freedom (DOF), that is surge, sway and yaw.

Assumption 2. The vessel is port-starboard symmetric.

Assumption 3. The body-fixed coordinate frame b is located on the center-line of the vessel at a distance x_g^* from the center of gravity (CG), where x_g^* is to be defined later.

Assumption 4. The hydrodynamic damping is linear.

B. The Ocean Current

The drifting effect of currents, tides, low frequency swells and second order wave-induced forces is embodied into the ocean current vector denoted as $\boldsymbol{V}_c$:

Assumption 5. The ocean current is defined in the inertial frame i and is assumed constant, unknown, irrotational and bounded. Hence, $\boldsymbol{V}_c \triangleq [V_x, V_y, 0]^T$ and there exists a constant $V_{\max} > 0$ such that $V_{\max} \geq \sqrt{V_x^2 + V_y^2}$.

Remark 1. The constant and irrotational ocean current model is widely accepted to describe slowly varying disturbances and it represents a good approximation when closed-loop control is implemented on-board of marine vehicles [19].

Remark 2. The first order wave-induced forces are neglected in this context since they cause zero mean oscillatory motions that are usually removed through wave filtering [16].

C. The Control Plant Model

The state of the surface vessel is given by the vector $[\boldsymbol{p}^T, \boldsymbol{\nu}_r^T]^T$ where $\boldsymbol{p} \triangleq [x, y, \psi]^T$ describes the position and the orientation of the vehicle with respect to the inertial frame i. The vector $\boldsymbol{\nu} \triangleq [u, v, r]^T$ contains the linear and angular velocities of the ship defined in the body-fixed frame b, where u is the surge velocity, v is the sway velocity and r is the yaw rate. The ocean current velocity in the body frame b, $\boldsymbol{\nu}_c \triangleq [u_c, v_c, 0]^T$, is obtained from $\boldsymbol{\nu}_c = \boldsymbol{R}^T(\psi)\boldsymbol{V}_c$ where $\boldsymbol{R}(\psi)$ is the rotation matrix from b to i. Following Assumption 5 the ocean current is constant and irrotational in i and hence $\dot{\boldsymbol{V}}_c = \boldsymbol{0}$, and $\dot{\boldsymbol{\nu}}_c = [rv_c, -ru_c, 0]^T$. When ocean currents are present it is useful to describe the state of the vessel with the relative velocity vector (i.e. velocity relative to water): $\boldsymbol{\nu}_r \triangleq \boldsymbol{\nu} - \boldsymbol{\nu}_c = [u_r, v_r, r]^T$. The vector $\boldsymbol{\nu}_r$ is defined in b, where u_r is the relative surge velocity and v_r is the relative sway velocity. This paper, under Assumption 5, covers the class of marine vehicles described by the following 3-DOF maneuvering model expressed in terms of $\boldsymbol{\nu}_r$ [10], [16]:

$$\dot{\boldsymbol{p}} = \boldsymbol{R}(\psi)\boldsymbol{\nu}_r + \boldsymbol{V}_c, \tag{1}$$

$$\boldsymbol{M}\dot{\boldsymbol{\nu}}_r + \boldsymbol{C}(\boldsymbol{\nu}_r)\boldsymbol{\nu}_r + \boldsymbol{D}\boldsymbol{\nu}_r = \boldsymbol{B}\boldsymbol{f} + \boldsymbol{w}. \tag{2}$$

Remark 3. The ocean current $\boldsymbol{V}_c$ does not depend on the heading of the vessel and represents a kinematic bias in (1). It defines in fact a constant and irrotational velocity drift and hence it does not capture the heading dependent disturbing effects of currents, wind and waves. In this paper the vector $\boldsymbol{w}$ is introduced in (2) to take into account for these disturbances as well. In particular, the significant effect of wind is analyzed in this context.

The vector $\boldsymbol{f} \triangleq [T_u, T_r]^T$ is the control input vector, containing the surge thrust T_u and the rudder angle T_r. Notice that the model (1-2) is underactuated in its configuration space since it has fewer control inputs than DOFs. The vector $\boldsymbol{w} \triangleq [w_u, w_v, w_r]^T$ is the body-fixed dynamic environmental load vector. The vector $\boldsymbol{w}$ is defined and discussed in detail in Section II-D. The matrix $\boldsymbol{M} = \boldsymbol{M}^T > 0$ is the mass and inertia matrix and includes hydrodynamic zero frequency added mass. The matrix $\boldsymbol{C}$ is the Coriolis and centripetal matrix, $\boldsymbol{D} > 0$ is the hydrodynamic damping matrix, assuming linear or linearized damping, and $\boldsymbol{B} \in \mathbb{R}^{3\times 2}$ is the actuator configuration matrix. For maneuvering control purposes, the matrices $\boldsymbol{R}(\psi)$, $\boldsymbol{M}$, $\boldsymbol{D}$, $\boldsymbol{B}$ are considered to have the following structures:

$$\boldsymbol{R}(\psi) \triangleq \begin{bmatrix} \cos(\psi) & -\sin(\psi) & 0 \\ \sin(\psi) & \cos(\psi) & 0 \\ 0 & 0 & 1 \end{bmatrix}, \quad \boldsymbol{M} \triangleq \begin{bmatrix} m_{11} & 0 & 0 \\ 0 & m_{22} & m_{23} \\ 0 & m_{23} & m_{33} \end{bmatrix}, \tag{3}$$

$$\boldsymbol{D} \triangleq \begin{bmatrix} d_{11} & 0 & 0 \\ 0 & d_{22} & d_{23} \\ 0 & d_{32} & d_{33} \end{bmatrix}, \quad \boldsymbol{B} \triangleq \begin{bmatrix} b_{11} & 0 \\ 0 & b_{22} \\ 0 & b_{32} \end{bmatrix}. \tag{4}$$

The particular structure of $\boldsymbol{M}$ and $\boldsymbol{D}$ is justified by Assumptions 1-4. The actuator configuration matrix $\boldsymbol{B}$ has full column rank and maps the control inputs T_u and T_r into forces and moments acting on the vessel. The Coriolis and centripetal matrix $\boldsymbol{C}$ is obtained from $\boldsymbol{M}$ as [16]:

$$\boldsymbol{C}(\boldsymbol{\nu}_r) \triangleq \begin{bmatrix} 0 & 0 & -m_{22}v_r - m_{23}r \\ 0 & 0 & m_{11}u_r \\ m_{22}v_r + m_{23}r & -m_{11}u_r & 0 \end{bmatrix}. \tag{5}$$

Finally, x_g^* from Assumption 3 is chosen so that $\boldsymbol{M}^{-1}\boldsymbol{B}\boldsymbol{f} = [\tau_u, 0, \tau_r]^T$. The point $(x_g^*, 0)$ exists for all port-starboard symmetric vehicles [10]. Notice that in (1-2) there are two terms describing environmental disturbances: the current $\boldsymbol{V}_c$ in (1), representing a pure kinematic drift, and the vector $\boldsymbol{w}$ in (2), representing heading dependent disturbances that show up at the dynamic level. The vector $\boldsymbol{w}$ is defined and discussed in the following Section II-D.

D. The Environmental Load Vector $\boldsymbol{w}$

The vector $\boldsymbol{w}$ represents a bias term that embodies unmodeled dynamics and heading-dependent disturbances caused by currents, winds and waves. In this context, the significant effect of constant wind disturbances is assumed to dominate in $\boldsymbol{w}$. Inspired by [15] and [16], the overall effect of wind is modeled as a constant pressure P_e acting on the vessel in a constant direction β_e:

Assumption 6. The pressure $P_e > 0$ is considered constant, unknown, and acting in a constant and known direction β_e of the inertial frame. Therefore, there exists a constant $P_e^{\max} > 0$ such that $P_e^{\max} \geq P_e$.

Remark 4. The mean and slowly varying drifting effect caused by wind is considered, while the peaks arising from wind gusts are neglected since they are often removed through filtering and feedforward. The direction β_e is assumed known since the tools to measure and estimate the wind direction are often available [16], [20].

The forces and moments generated by the wind pressure P_e on the ship are proportional to the frontal and lateral projected areas above the waterline of the ship, and to some well-defined load coefficients. The areas above the waterline are considered since the effect of wind is limited to the surface. The loading coefficients depend on the geometry of the ship hull and superstructure, and are functions of the disturbance angle of attack. They are usually obtained through interpolation of data from simulations and wind tunnel tests for different types of ships [15], [21], [22]. The environmental load vector $\boldsymbol{w}$ is then defined as:

$$\boldsymbol{w} \triangleq \begin{bmatrix} P_e A_{Fw} C_X(\gamma_e) \\ P_e A_{Lw} C_Y(\gamma_e) \\ P_e A_{Lw} L_{oa} C_N(\gamma_e) \end{bmatrix}, \tag{6}$$

where A_{Fw} is the frontal projected area above the waterline, A_{Lw} is the lateral projected area above the waterline, and L_{oa} is the length overall of the vessel (maximum length of the vessel hull). The term $\gamma_e \triangleq \psi - \beta_e - \pi$ is the angle of attack of the wind. The terms $C_X(\gamma_e)$, $C_Y(\gamma_e)$ and $C_N(\gamma_e)$ are the load coefficients. The following assumption is introduced:

Assumption 7. There are no dynamic disturbances in sway and yaw in presence of head/following sea ($\gamma_e = n\pi$, i.e. multiples of 0 and π) and no dynamic disturbances in surge in presence of beam sea ($\gamma_e = \pi/2 \pm n\pi$, i.e. multiples of $\pi/2$ and $2\pi/3$).

The load coefficients can be then redefined as: $C_X(\gamma_e) \triangleq C_X^*(\gamma_e)\cos(\gamma_e)$, $C_Y(\gamma_e) \triangleq C_Y^*(\gamma_e)\sin(\gamma_e)$ and $C_N(\gamma_e) \triangleq C_N^*(\gamma_e)\sin(\gamma_e)$. The vector $\boldsymbol{w}$ is rewritten as:

$$\boldsymbol{w} = \begin{bmatrix} -P_e A_{Fw} C_X^*(\gamma_e)\cos(\beta_e - \psi) \\ P_e A_{Lw} C_Y^*(\gamma_e)\sin(\beta_e - \psi) \\ P_e A_{Lw} L_{oa} C_N^*(\gamma_e)\sin(\beta_e - \psi) \end{bmatrix}. \tag{7}$$

Furthermore, the functions $C_X^*(\gamma_e)$, $C_Y^*(\gamma_e)$ and $C_N^*(\gamma_e)$ are required to satisfy:

Assumption 8. $C_X^*(\gamma_e)$, $C_Y^*(\gamma_e)$, $C_N^*(\gamma_e)$ are bounded, periodic, class C^1 functions with bounded first derivatives and satisfy:

- $C_X^*(\gamma_e) < 0, \quad \forall\ \gamma_e$,
- $C_Y^*(\gamma_e) > 0, \quad \forall\ \gamma_e$,
- $-m_{23} C_Y^*(\gamma_e) + m_{22} L_{oa} C_N^*(\gamma_e) \neq 0$ for $\gamma_e = \pi/2 \pm n\pi$.

Finally, the following function is considered:

$$\kappa_v(\cdot) \triangleq \frac{P_e A_{Lw}}{m_{22} m_{33} - m_{23}^2} \left[m_{33} C_Y^*(\cdot) - m_{23} L_{oa} C_N^*(\cdot) \right]. \tag{8}$$

Since $C_Y^*(\cdot)$ and $C_N^*(\cdot)$ are bounded,they have bounded first derivatives and P_e is bounded, then there exist $\kappa_v^{\max}, \kappa_v'^{\max} > 0$ such that $\kappa_v(\cdot) \leq \kappa_v^{\max}$, $\frac{d\kappa_v(\cdot)}{d\cdot} \leq \kappa_v'^{\max}$.

Assumption 9. $C_Y^*(\cdot)$ and $C_N^*(\cdot)$ are such that, given any constants $k \in \mathbb{R}$ and $\beta_e \in [0, 2\pi]$, the following bound holds for all $s \in \mathbb{R}$:

$$\left| \kappa_v(\gamma_e^k) - \kappa_v(\gamma_e^{k+s}) \frac{\sqrt{k^2+1}}{\sqrt{(s+k)^2+1}} \right| \leq \kappa_v^{\max} \frac{|s|}{\sqrt{(s+k)^2+1}}, \tag{9}$$

where $\gamma_e^k \triangleq -\tan^{-1}(k) - \beta_e - \pi$ and $\gamma_e^{k+s} \triangleq -\tan^{-1}(k+s) - \beta_e - \pi$.

Remark 5. Notice that the wind load coefficients given in [15], [16], [21], [22] trivially satisfy Assumptions 7-9, or can be easily approximated with functions satisfying Assumptions 7-9.

Remark 6. Given the model (1-2) one can choose to consider both the proposed disturbances, $[V_x, V_y, 0]^T$ and $\boldsymbol{w}$, or only one, depending on the application, type of vessel and the environmental conditions.

E. The Model in Component Form

To solve nonlinear underactuated control design problems it is useful to expand the model (1-2) into a component form:

$$\dot{x} = u_r \cos(\psi) - v_r \sin(\psi) + V_x, \tag{10a}$$
$$\dot{y} = u_r \sin(\psi) + v_r \cos(\psi) + V_y, \tag{10b}$$
$$\dot{\psi} = r, \tag{10c}$$
$$\dot{u}_r = F_u(u_r, v_r, r) + P_e \kappa_u^*(\gamma_e)\cos(\beta_e - \psi) + \tau_u, \tag{10d}$$
$$\dot{v}_r = X(u_r) r + Y(u_r) v_r + \kappa_v(\gamma_e)\sin(\beta_e - \psi), \tag{10e}$$
$$\dot{r} = F_r(u_r, v_r, r) + P_e \kappa_r^*(\gamma_e)\sin(\beta_e - \psi) + \tau_r. \tag{10f}$$

Notice the absence of any control inputs in sway (10e) to compensate for the environmental disturbances. The ship should therefore crab to counteract for currents, wind and waves having abeam components. The expressions for $\kappa_u^*(\gamma_e)$, $\kappa_r^*(\gamma_e)$, $F_r(u_r, v_r, r)$, $F_u(v_r, r)$, $X(u_r)$ and $Y(u_r)$ are given in Appendix I. Furthermore, the functions $Y(u_r)$ and $X(u_r)$ are bounded for bounded arguments and thus satisfy the following assumption:

Assumption 10. $Y(u_r)$ satisfies $Y(u_r) \leq -Y^{\min} < 0, \quad \forall u_r \in [-V_{\max}, U_{rd}]$, where $Y^{\min}$ is a positive constant.

Remark 7. Assumption 10 is justified by a contradiction: $Y(u_r) \geq 0$ would imply a nominally unstable vehicle in sway which is not the case for commercial vessels by design. No bounds are implied on u_r and $U_{rd} > 0$ is defined in the next section.

III. Control Objective

The control system should make the vessel follow a given straight line $\mathcal{P}$ and maintain a desired constant surge relative velocity $U_{rd} > 0$ in the presence of environmental disturbances, modeled as a combination of the ocean current $\boldsymbol{V}_c$ and the wind pressure P_e. The inertial reference frame i is placed such that x-axis is aligned with the desired path $\mathcal{P}$ as shown in Fig. 1 without any loss of generality, giving $\mathcal{P} \triangleq \{(x, y) \in \mathbb{R}^2 : y = 0\}$. The vehicle y coordinate then corresponds to the horizontal cross-track error and the control objectives become:

$$\lim_{t\to\infty} y(t) = 0, \tag{11}$$
$$\lim_{t\to\infty} \psi(t) = \psi_{ss}, \tag{12}$$
$$\lim_{t\to\infty} u_r(t) = U_{rd}, \tag{13}$$

where $\psi_{ss} \in (-\pi/2, \pi/2)$ is constant. The yaw angle $\psi(t)$ is not required to converge to zero but rather to a steady-state constant value to make the vessel crab and thus

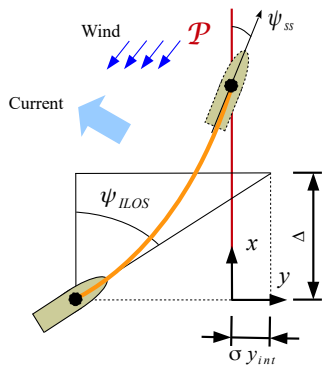

Fig. 1. Integral line of sight guidance for an underactuated surface vessel. At steady state the nonzero angle ψ_{ss} allows the underactuated vehicle to counteract the disturbances.

counteract the environmental disturbances since the ship is underactuated and no control forces are available in sway to compensate for the drift. The value of ψ_{ss} will be specified later. The relative velocity needs to be sufficiently large to guarantee ship maneuverability in presence of disturbances. In particular, it is shown in this paper that the following assumption guarantees path following in presence of kinematic and dynamic disturbances acting in any direction:

Assumption 11. U_{rd} satisfies the following condition:

$$U_{rd} > \max\left\{V_{\max} + \frac{5}{2}\left|\frac{\kappa_v^{\max}}{Y(U_{rd})}\right|, 2V_{\max} + 2\left|\frac{\kappa_v^{\max} + \kappa_v'^{\max}}{Y(U_{rd})}\right|\right\}.$$

Remark: It is always possible to find values of U_{rd} satisfying Assumption 11, since $|Y(u_r)|$ is strictly increasing for $u_r > 0$.

Remark: The chosen control approach is based on relative velocities: see [10] for more details on relative vs absolute velocity.

IV. The Integral Line of Sight Guidance

The ILOS guidance is introduced in a cascaded configuration with adaptive surge and yaw controllers to solve the path following problem described in Section III. The surface vessel has to converge and follow the x-axis in presence of environmental disturbances. In this paper it is shown that the ILOS guidance method introduced in [9] in combination with adaptive surge and yaw controllers compensates for both kinematic as well as dynamic disturbances, further extending the results of [10], [14]. Hence, the desired heading angle is:

$$\psi_{ILOS} \triangleq -\tan^{-1}\left(\frac{y + \sigma y_{\text{int}}}{\Delta}\right), \qquad \Delta, \sigma > 0, \tag{14a}$$

$$\dot{y}_{\text{int}} = \frac{\Delta y}{(y + \sigma y_{\text{int}})^2 + \Delta^2}, \tag{14b}$$

where Δ is the look-ahead distance, and σ is the integral gain, both constant design parameters. A detailed description of the ILOS guidance law is given in [10].

V. The Surge and Yaw Controllers

This section presents the adaptive surge-yaw controller that, added in a cascaded configuration with the ILOS guidance from Section IV, solves the tasks defined in Section III when the wind pressure P_e is unknown.

Remark 8. An adaptive version for the surge and yaw controllers is presented to add robustness with respect to the unknown dynamic disturbance P_e. In fact, it is common to have both feed-forward and integral action in modern autopilots and speed controllers [16].

The following combined surge-yaw controller is proposed:

$$\begin{aligned}\tau_u =& -F_{u_r}(u_r, v_r, r) + \dot{u}_{rd} - k_{u_r}(u_r - u_{rd}) \\ & - \hat{P}_e \kappa_u^*(\gamma_e)\cos(\beta_e - \psi),\end{aligned} \tag{15a}$$

$$\begin{aligned}\tau_r =& -F_r(u_r, v_r, r) + \ddot{\psi}_d - (k_\psi + \lambda k_r)(\psi - \psi_d) \\ & - (k_r + \lambda)(\dot{\psi} - \dot{\psi}_d) - \hat{P}_e \kappa_r^*(\gamma_e)\sin(\beta_e - \psi),\end{aligned} \tag{15b}$$

$$\dot{\hat{P}}_e = \gamma_1 \boldsymbol{G}^T(\psi)\begin{bmatrix} u_r - u_{rd} \\ \gamma_2(\psi - \psi_d) \\ \gamma_2[(\dot{\psi} - \dot{\psi}_d) + \lambda(\psi - \psi_d)] \end{bmatrix}, \tag{15c}$$

where $\boldsymbol{G}(\psi) \triangleq [\kappa_u^*(\gamma_e)\cos(\beta_e - \psi) \quad 0 \quad \kappa_r^*(\gamma_e)\sin(\beta_e - \psi)]^T$ is the regressor, $k_{u_r}, k_\psi, k_r, \lambda > 0$ are constant controller gains and $\gamma_1, \gamma_2 > 0$ are constant adaption gains. The controller (15) is an adaptive feedback linearizing controller and, as later shown in Section VII, it makes sure that u_r, ψ and r exponentially track u_{rd}, ψ_d and $\dot{\psi}_d$. The generic references u_{rd} and ψ_d are set to U_{rd} and ψ_{ILOS} respectively, in the following sections. Furthermore, $\hat{P}_e$ exponentially estimates the magnitude of the unknown disturbance P_e.

VI. Stability Conditions

This section presents the stability conditions under which the proposed ILOS guidance (14) in a cascaded configuration with the adaptive controller (15) achieves the objectives (11-13). The notation $X^{U_{rd}} \triangleq X(U_{rd})$, $Y^{U_{rd}} \triangleq Y(U_{rd})$ is used.

Theorem 1. *Given an underactuated surface vessel described by the dynamical system (10). If Assumptions 5-11 hold and, if the look-ahead distance Δ and the integral gain σ satisfy the conditions:*

$$\Delta > \frac{|X^{U_{rd}}|}{|Y^{U_{rd}}|}\Omega(\sigma)\left[\frac{5}{4}\frac{U_{rd} + V_{\max} + \sigma}{U_{rd} - V_{\max} - \sigma} + 1\right], \tag{16}$$

$$0 < \sigma < U_{rd} - V_{\max} - \frac{5}{2}\left|\frac{\kappa_v^{\max}}{Y^{U_rd}}\right|, \tag{17}$$

where $\Omega(\sigma)$ is defined as,

$$\Omega(\sigma) \triangleq \frac{U_{rd} - V_{\max} - \sigma}{U_{rd} - V_{\max} - \sigma - \frac{5}{2}\left|\frac{\kappa_v^{\max}}{Y^{U_rd}}\right|}, \tag{18}$$

then the controller (15)*, where ψ_d is given by* (14) *and $u_{rd} \triangleq U_{rd}$, guarantee achievement of the control objectives (11-13).*

VII. Proof of Theorem 1

The first part of the proof follows along the line of [10]. The dynamics of the cross track error y and the relative sway velocity v_r are analyzed first. Given the error signals $\tilde{u}_r \triangleq u_r - U_{rd}$, $\tilde{\psi} \triangleq \psi - \psi_d$, $\tilde{\dot{\psi}} \triangleq r - \dot{\psi}_d$, the vector

$\boldsymbol{\zeta} \triangleq [\tilde{u}_r, \tilde{\psi}, \dot{\tilde{\psi}}]^T$ is defined. Combining (10b), (10e) and (14b) leads to the $y - v_r$ subsystem that is analyzed in [10]:

$$\dot{y}_{\text{int}} = \frac{\Delta y}{(y + \sigma y_{\text{int}})^2 + \Delta^2}, \tag{19a}$$

$$\dot{y} = (\tilde{u}_r + U_{rd}) \sin(\tilde{\psi} + \psi_d) + v_r \cos(\tilde{\psi} + \psi_d) + V_y, \tag{19b}$$

$$\begin{aligned}\dot{v}_r =& X(\tilde{u}_r + U_{rd})(\dot{\tilde{\psi}} + \dot{\psi}_d) + Y(\tilde{u}_r + U_{rd})v_r \\ &+ \kappa_v(\gamma_e) \sin(\beta_e - \tilde{\psi} - \psi_d).\end{aligned} \tag{19c}$$

The equilibrium point of the system (19) on the manifold $\boldsymbol{\zeta} = [\tilde{u}_r, \tilde{\psi}, \dot{\tilde{\psi}}]^T = \mathbf{0}$ is given by the following equation:

$$s\sqrt{s^2+1} = \frac{V_y}{U_{rd}} s^2 + \frac{\cos(\beta_e)s + \sin(\beta_e)}{U_{rd}|Y^{U_{rd}}|} \kappa_v^{\text{eq}}(s) + \frac{V_y}{U_{rd}}, \tag{20}$$

where $s \triangleq \sigma y_{\text{int}}^{\text{eq}}/\Delta$ and $y_{\text{int}}^{\text{eq}}$ is the value of y_{int} at equilibrium. The term $\kappa_v^{\text{eq}}(s)$ is defined as the value of $\kappa_v(\gamma_e)$ at equilibrium, i.e. when $\gamma_e = \gamma_e^{\text{eq}} \triangleq -\tan^{-1}(s) - \beta_e - \pi$. The equilibrium point equation (20) is assessed in [10] where it is shown under which conditions (20) has a unique real solution, hence a single equilibrium point:

Lemma 1. *If Assumptions 8 and 11 hold, then* (20) *has exactly one real solution* $s = \sigma y_{\text{int}}^{\text{eq}}/\Delta$.

Proof. The proof of Lemma 1 is given in [10, Lemma 1]. □

At equilibrium $y^{\text{eq}} = 0$ while $y_{\text{int}}^{\text{eq}}$ and v_r^{eq} are constant values where $y_{\text{int}}^{\text{eq}}$ is the unique solution of (20) and v_r^{eq} relates to $y_{\text{int}}^{\text{eq}}$ as $v_r^{\text{eq}} = U_{rd}\sigma y_{\text{int}}^{\text{eq}}/\Delta - V_y\sqrt{(\sigma y_{\text{int}}^{\text{eq}}/\Delta)^2 + 1)}$. The heading angle held by the vessel at steady-state is then $\psi_{ss} \triangleq -\tan^{-1}(\sigma y_{\text{int}}^{\text{eq}}/\Delta)$. A new set of variables is introduced to move the equilibrium point to the origin: $e_1 \triangleq y_{\text{int}} - y_{\text{int}}^{\text{eq}}$, $e_2 \triangleq y + \sigma e_1$ and $e_3 \triangleq v_r - v_r^{\text{eq}}$. Substituting (14a) for ψ_d and factorizing the result with respect to $\boldsymbol{\zeta}$ leads (19) to the following expression:

$$\begin{bmatrix} \dot{e_1} \\ \dot{e_2} \\ \dot{e_3} \end{bmatrix} = \boldsymbol{A}(e_2) \begin{bmatrix} e_1 \\ e_2 \\ e_3 \end{bmatrix} + \boldsymbol{B}(e_2) + \boldsymbol{H}(y, y_{\text{int}}, \psi_d, v_r, \boldsymbol{\zeta})\boldsymbol{\zeta}. \tag{21}$$

The term $\boldsymbol{H}$ contains all the terms vanishing at $\boldsymbol{\zeta} = \mathbf{0}$. $\boldsymbol{A}$ is given in (30) while $\boldsymbol{B}$ and $\boldsymbol{H}$ are:

$$\boldsymbol{B}(e_2) \triangleq \begin{bmatrix} 0 \\ V_y f(e_2) \\ -\frac{\Delta X^{U_{rd}} V_y}{(e_2 + \sigma y_{\text{int}}^{\text{eq}})^2 + \Delta^2} f(e_2) + \sin(\psi_{ss} - \beta_e) g(e_2) \end{bmatrix}, \tag{22}$$

$$\boldsymbol{H}(y, y_{\text{int}}, \psi_d, v_r, \boldsymbol{\zeta}) \triangleq \begin{bmatrix} 0 & 0 \\ 1 & 0 \\ -\frac{\Delta X(\tilde{u}_r + U_{rd})}{(e_2 + \sigma y_{\text{int}}^{\text{eq}})^2 + \Delta^2} & 1 \end{bmatrix} \begin{bmatrix} \boldsymbol{h}_y^T \\ \boldsymbol{h}_{v_r}^T \end{bmatrix}, \tag{23}$$

and

$$f(e_2) \triangleq 1 - \frac{\sqrt{(\sigma y_{\text{int}}^{\text{eq}})^2 + \Delta^2}}{\sqrt{(e_2 + \sigma y_{\text{int}}^{\text{eq}})^2 + \Delta^2}}, \tag{24}$$

$$g(e_2) \triangleq \kappa_v^{\text{eq}} - \frac{\kappa_v(\gamma_e)\sqrt{(\sigma y_{\text{int}}^{\text{eq}})^2 + \Delta^2}}{\sqrt{(e_2 + \sigma y_{\text{int}}^{\text{eq}})^2 + \Delta^2}}. \tag{25}$$

The vectors $\boldsymbol{h}_y$ and $\boldsymbol{h}_{v_r}$ are given in Appendix I. The system (21) on the manifold $\boldsymbol{\zeta} = \mathbf{0}$ is equivalent to the following nominal system that is analyzed in [10]:

$$\begin{bmatrix} \dot{e_1} \\ \dot{e_2} \\ \dot{e_3} \end{bmatrix} = \boldsymbol{A}(e_2) \begin{bmatrix} e_1 \\ e_2 \\ e_3 \end{bmatrix} + \boldsymbol{B}(e_2). \tag{26}$$

Lemma 2 states the stability properties of (26):

Lemma 2. *Under the conditions of Theorem 1, the nominal system* (26) *is UGAS and ULES.*

Proof. The proof of Lemma 2 is given in [10, Lemma 2]. □

From this point on the proof differs substantially from [10] since the actuated dynamics (10d) and (10f) of the ship in closed loop configuration with the novel adaptive controller (15) are analyzed. Given the error signals $\tilde{u}_r$, $\tilde{\psi}$, $\epsilon \triangleq \dot{\tilde{\psi}} + \lambda\tilde{\psi}$ and the estimation error $\tilde{P}_e \triangleq P_e - \hat{P}_e$, the vector $\boldsymbol{\xi} \triangleq [\tilde{u}_r, \tilde{\psi}, \epsilon]^T$ is defined. The dynamics of $\boldsymbol{\xi}$ and $\tilde{P}_e$ are obtained by combining equations (10c), (10d), (10f) with (15):

$$\dot{\boldsymbol{\xi}} = \chi(\boldsymbol{\xi}) + \boldsymbol{G}(\tilde{\psi} + \psi_d(\boldsymbol{\xi}, t))\tilde{P}_e, \tag{27a}$$

$$\dot{\tilde{P}}_e = -\gamma_1 \boldsymbol{G}^T(\tilde{\psi} + \psi_d(\boldsymbol{\xi}, t)) \left[\frac{\partial W_1(\boldsymbol{\xi})}{\partial \boldsymbol{\xi}}\right]^T, \tag{27b}$$

where:

$$\chi(\boldsymbol{\xi}) \triangleq \begin{bmatrix} -k_{u_r} & 0 & 0 \\ 0 & -\lambda & 1 \\ 0 & -k_\psi & -k_r \end{bmatrix} \boldsymbol{\xi}, \tag{28}$$

$$W_1(\boldsymbol{\xi}) \triangleq \frac{1}{2}\tilde{u}_r^2 + \frac{\gamma_2 k_\psi}{2}\tilde{\psi}^2 + \frac{\gamma_2}{2}\epsilon^2. \tag{29}$$

The stability properties of the origin $(\mathbf{0}, 0)$ of (27) are assessed using [18, Theorem 1]. Assumption A2 of [18, Theorem 1] is considered first. In particular, notice that it is trivial to find three constants $c_1, c_2, c_3 > 0$ such that $c_1 \parallel \boldsymbol{\xi} \parallel \leq W_1(\boldsymbol{\xi}) \leq c_2 \parallel \boldsymbol{\xi} \parallel$ and $[\partial W_1(\boldsymbol{\xi})/\partial \boldsymbol{\xi}]\ \chi(\boldsymbol{\xi}) \leq -c_3 \parallel \boldsymbol{\xi} \parallel$. This satisfies Assumption A2 of [18, Theorem 1].

Assumption A1 of [18, Theorem 1] is considered next. Notice that the regressor $\boldsymbol{G}(\tilde{\psi} + \psi_d(\boldsymbol{\xi}, t))$ relies on the error signal $\tilde{\psi}$ and the reference $\psi_d(\boldsymbol{\xi}, t)$ to estimate the unknown P_e, where the reference $\psi_d(\boldsymbol{\xi}, t)$ is allowed to depend upon $\boldsymbol{\xi}$ as well. According to [18, Theorem 1] the regressor $\boldsymbol{G}(\tilde{\psi} + \psi_d(\boldsymbol{\xi}, t))$ has to be analyzed on the manifold $\boldsymbol{\xi} = \mathbf{0}$ (notice that $\boldsymbol{\xi} = \mathbf{0}$ implies $\boldsymbol{\zeta} = \mathbf{0}$). The notation $\psi_d^0 \triangleq \psi_d(\mathbf{0}, t)$ and $\boldsymbol{G}_0(\psi_d^0(t)) \triangleq \boldsymbol{G}(\tilde{\psi} + \psi_d(\boldsymbol{\xi}, t))|_{\boldsymbol{\xi} \equiv \mathbf{0}}$ is introduced for this purpose. Furthermore, some preliminary analysis of ψ_d^0 and its time derivative $\dot{\psi}_d^0 = \rho(y_{\text{int}}(t), y(t), v_r(t))|_{\boldsymbol{\xi} \equiv \mathbf{0}}$, where $\rho(y_{\text{int}}, y, v_r)$ is given in Appendix I, is necessary:

Corollary 1. ψ_d^0 and $\dot{\psi}_d^0$ are bounded and continuous.

Proof. The signal $\psi_d(t) = -\tan^{-1}[(y(t) + \sigma y_{\text{int}}(t))/\Delta]$ is function of the time trajectories $[e_1(t), e_2(t), e_3(t), \boldsymbol{\xi}^T(t), \tilde{P}_e(t)]^T$ as suggested by (21). However, the condition $\boldsymbol{\xi} = \mathbf{0}$ required by [18, Theorem 1] and that defines ψ_d^0, opens the loop. In fact, $\psi_d^0 = -\tan^{-1}[(y(t) + \sigma y_{\text{int}}(t))/\Delta]|_{\boldsymbol{\xi} \equiv \mathbf{0}}$ is function of the time trajectories $[e_1(t), e_2(t), e_3(t)]^T|_{\boldsymbol{\xi} \equiv \mathbf{0}}$ generated by the nominal system (26). Following Lemma 2, the nominal system (26) is UGAS and ULES, and therefore, the ψ_d^0 and $\dot{\psi}_d^0$ are always bounded and continuous. □

It is now possible to check that all the conditions of Assumption A1 in [18, Theorem 1] are satisfied. First, notice that it is trivial to find a continuous non-decreasing function $\theta_1(\cdot)$ such that

$$\boldsymbol{A}(e_2) \triangleq \begin{bmatrix} -\frac{\sigma\Delta}{(e_2+\sigma y_{\text{int}}^{\text{eq}})^2+\Delta^2} & \frac{\Delta}{(e_2+\sigma y_{\text{int}}^{\text{eq}})^2+\Delta^2} & 0 \\ -\frac{\sigma^2\Delta}{(e_2+\sigma y_{\text{int}}^{\text{eq}})^2+\Delta^2} & \Big(-\frac{U_{rd}}{\sqrt{(e_2+\sigma y_{\text{int}}^{\text{eq}})^2+\Delta^2}}+\frac{\sigma\Delta}{(e_2+\sigma y_{\text{int}}^{\text{eq}})^2+\Delta^2}\Big) & \frac{\Delta}{\sqrt{(e_2+\sigma y_{\text{int}}^{\text{eq}})^2+\Delta^2}} \\ \frac{\sigma^2\Delta^2 {X^U}_{rd}}{((e_2+\sigma y_{\text{int}}^{\text{eq}})^2+\Delta^2)^2} & \Big(\frac{{U_{rd}}\Delta {X^U}_{rd}}{((e_2+\sigma y_{\text{int}}^{\text{eq}})^2+\Delta^2)^{3/2}}-\frac{\sigma\Delta^2 {X^U}_{rd}}{((e_2+\sigma y_{\text{int}}^{\text{eq}})^2+\Delta^2)^2}+\frac{\kappa_v(\gamma_e)\cos(\beta_e)}{\sqrt{(e_2+\sigma y_{\text{int}}^{\text{eq}})^2+\Delta^2}}\Big) & \Big({Y^U}_{rd}-\frac{\Delta^2 {X^U}_{rd}}{((e_2+\sigma y_{\text{int}}^{\text{eq}})^2+\Delta^2)^{3/2}}\Big) \end{bmatrix} \tag{30}$$

$\max\{\| \chi(\boldsymbol{\xi}) \|, \| \partial W_1(\boldsymbol{\xi})/\partial\boldsymbol{\xi} \|\} \leq \theta_1(\| \boldsymbol{\xi} \|) \| \boldsymbol{\xi} \|$. Next, since $\boldsymbol{G}(\cdot)$ is globally bounded, it is straightforward to find a continuous non-decreasing function $\theta_2(\cdot)$ satisfying the inequality $\max\{\| \boldsymbol{G}(\tilde{\psi}+\psi_d(\boldsymbol{\xi},t)) \|, \| \boldsymbol{G}_0(\psi_d^0(t)) \|\} \leq \theta_2(\| [\boldsymbol{\xi}^T, \tilde{P}_e]^T \|)$. Furthermore, Assumption 8 guarantees that there exists a constant $b_m > 0$ such that $\boldsymbol{G}(\cdot)^T\boldsymbol{G}(\cdot) \geq b_m$, regardless of the argument. Therefore, conditions (9) (10) and (12) in Assumption A1 of [18, Theorem 1] are satisfied. Finally, the partial derivative $\partial\boldsymbol{G}_0(\psi_d^0)/\partial\tilde{P}_e$ and the time derivative $\partial\boldsymbol{G}_0(\psi_d^0)/\partial t$ are analyzed to show that condition (11) in [18, Theorem 1] is fulfilled. In particular, $\partial\boldsymbol{G}_0(\psi_d^0)/\partial\tilde{P}_e = 0$, while $\partial\boldsymbol{G}_0(\psi_d^0)/\partial t$ can be rewritten as $\partial\boldsymbol{G}_0(\psi_d^0)/\partial t = (\partial\boldsymbol{G}_0(\psi_d^0)/\partial\psi_d^0)\dot{\psi}_d^0$. Assumption 8 makes sure that $\partial\boldsymbol{G}_0(\psi_d^0)/\partial\psi_d^0$ is well defined and bounded, while continuity and boundedness of $\dot{\psi}_d^0$ is shown by Corollary 1. Thus, the time derivative $\partial\boldsymbol{G}_0(\psi_d^0)/\partial t$ is bounded and there exists a non-decreasing function $\theta_3(\cdot)$ such that $\max\{\| \partial W_1(\boldsymbol{\xi})/\partial\tilde{P}_e \|, \| \partial\boldsymbol{G}_0(\psi_d^0(t))/\partial t \|\} \leq \theta_3(|\tilde{P}_e|)$. This fulfills condition (11) in Assumption A1 of [18, Theorem 1]. All the assumptions of [18, Theorem 1] are thus satisfied and it is therefore possible to conclude UGAS and ULES for the origin of the system (27). Therefore the control goal (13) is achieved with exponential converging properties in any ball of initial conditions. Finally, the interconnected dynamics of (19) and (27) are considered. The complete cascaded system of (19) and (27) is given by:

$$\begin{bmatrix} \dot{e_1} \\ \dot{e_2} \\ \dot{e_3} \end{bmatrix} = \boldsymbol{A}(e_2)\begin{bmatrix} e_1 \\ e_2 \\ e_3 \end{bmatrix} + \boldsymbol{B}(e_2) + \boldsymbol{H}(y, y_{\text{int}}, \psi_d, v_r, \boldsymbol{\Lambda\xi})\boldsymbol{\Lambda\xi}, \tag{31a}$$

$$\dot{\boldsymbol{\xi}} = \chi(\boldsymbol{\xi}) + \boldsymbol{G}(\tilde{\psi}+\psi_d)\tilde{P}_e, \tag{31b}$$

$$\dot{\tilde{P}}_e = -\gamma_1\boldsymbol{G}^T(\tilde{\psi}+\psi_d)\left[\frac{\partial W_1(\boldsymbol{\xi})}{\partial\boldsymbol{\xi}}\right]^T, \quad \boldsymbol{\Lambda} \triangleq \begin{bmatrix} 1 & 0 & 0 \\ 0 & 1 & 0 \\ 0 & -\lambda & 1 \end{bmatrix}, \tag{31c}$$

where $\boldsymbol{\zeta} = \boldsymbol{\Lambda\xi}$, with $\boldsymbol{\Lambda} > 0$ non-singular. Notice that the system (31) is a cascaded system, where the subsystem (31b-31c) perturbs the dynamics (31a) through the interconnection matrix $\boldsymbol{H}$. The perturbing system (31b-31c) is UGAS and ULES and the interconnection matrix $\boldsymbol{H}$ can be shown to satisfy $\| \boldsymbol{H} \| \leq \theta_4(\| \boldsymbol{\zeta} \|)(|y|+|y_{\text{int}}|+|v_r|)+\theta_5(\| \boldsymbol{\zeta} \|)$ where $\theta_4(\cdot)$ and $\theta_5(\cdot)$ are some continuous non-negative functions. Therefore, applying [23, Theorem 2] and [24, Lemma 8] concludes that under the conditions of Theorem 1 the origin $(e_1, e_2, e_3, \boldsymbol{\xi}, \tilde{P}_e) = (0, 0, 0, \boldsymbol{0}, 0)$ of the system (31) is UGAS and ULES, or alternatively, globally κ-exponentially stable. Hence, the objectives (11-12) are achieved with exponential converging properties in any ball of initial conditions and $\psi_{ss} = -\tan^{-1}(\sigma y_{\text{int}}^{\text{eq}}/\Delta)$.

VIII. Simulations

The supply ship model from [25] is used with the following improved linear damping matrix for maneuvering simulation purposes:

$$\boldsymbol{D} = \begin{bmatrix} 1.74{\cdot}10^5[\text{kg/s}] & 0 & 0 \\ 0 & 1.25{\cdot}10^6[\text{kg/s}] & 2.14{\cdot}10^6[\text{kg m/s}] \\ 0 & -6.24{\cdot}10^7[\text{kg m/s}] & 1.35{\cdot}10^9[\text{kg/s}^2] \end{bmatrix}. \tag{32}$$

Notice that $\boldsymbol{D} > 0$ and is obtained from linearization of more complex nonlinear damping models about the mean speed U_{rd}. The objective is to make the vessel follow the path $\mathcal{P}$ with a desired surge relative velocity $U_{rd} = 6$ [m/s] in presence of both ocean currents and wind disturbances. The intensity of the current is $|\boldsymbol{V}_c| = 0.9$ [m/s] and its components are $V_x = -0.17$ [m/s] and $V_y = 0.88$ [m/s], having a direction of 100.7 [deg]. Thus, Assumption 5 is fulfilled with $V_{\max} = 1$ [m/s] and it can be verified that Assumption 10 is satisfied with $Y_{\min} = 0.039$ [s^{-1}]. The upper limit for the wind pressure P_e is set to $P_e^{\max} = 570$ [N/m^2]. It corresponds approximately to the dynamic pressure generated by wind having 30 [m/s] of speed at the temperature of 10 [C°]. This is a reasonable upper limit since most offshore operations will not be carried out in such harsh conditions. The pressure P_e and its direction β_e are set to $P_e = 139.25$ [N/m^2] and $\beta_e = 196.9$ [deg]. Notice that the two disturbances act in different directions. The wind load coefficients for the offshore supply vessel case from [15] satisfy Assumption 7 and are chosen to define $C_X^*(\gamma_e), C_Y^*(\gamma_e), C_N^*(\gamma_e)$. Notice that $C_X^*(\gamma_e), C_Y^*(\gamma_e), C_N^*(\gamma_e)$ are smoothened with the functions $\text{trg}_{\pi,\text{smooth}}$ and $\text{sqr}_{\text{smooth}}$ from Appendix I to become class C^1 functions with bounded first derivatives. Hence, it is possible to verify that Assumptions 8-9 are verified

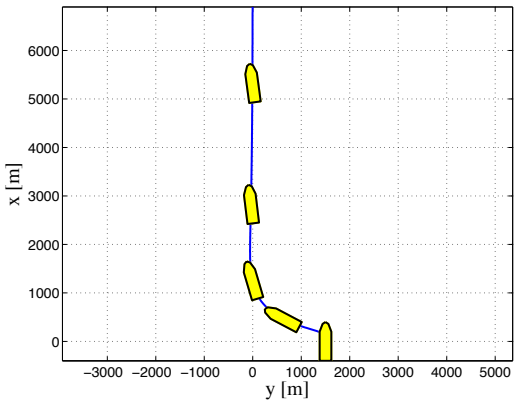

Fig. 2. Simulation of convergence and path following of the supply vessel in presence of multiple disturbances (time interval $0 - 1400$ [s]).

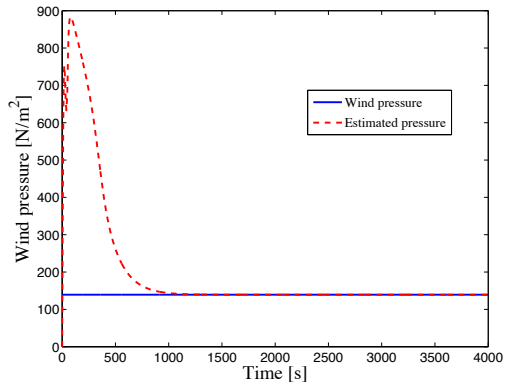

Fig. 3. Adaptive surge-yaw controller estimate $\hat{P}_e(t)$ from simulations. In this case $V_x = -0.17$ [m/s], $V_y = 0.88$ [m/s], $P_e = 139.25$ [N/m^2] and $\beta_e = 196.9$ [deg]. The steady state attack angle is $\gamma_e^{\text{eq}} \approx -24.8$ [deg].

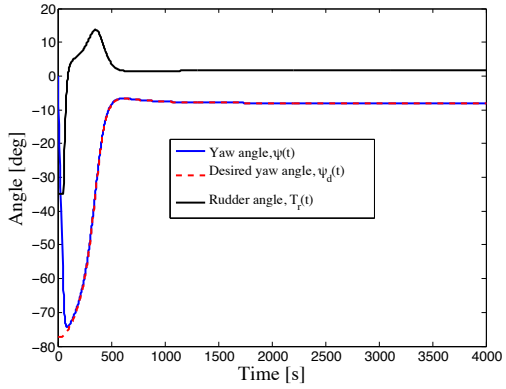

Fig. 4. Yaw angle $\psi(t)$ of the supply ship from simulations. Notice the side-slip angle $\psi_{ss} \approx -8.0$ [deg] in steady state.

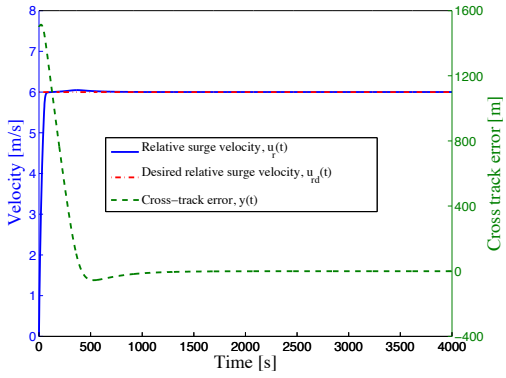

Fig. 5. Cross-track error $y(t)$ and relative surge velocity $u_r(t)$ of the vessel from simulations. Notice the overshoots caused by integral action.

with $\kappa_v^{\max} = 0.036$ [m/s^2] and $\kappa_v'^{\max} = 0.02$ [m/s^2]. Furthermore, the frontal and lateral projected areas above the waterline of the supply vessel in [25] are estimated as $A_{Fw} = 282.00$ [m^2] and $A_{Lw} = 554.90$ [m^2], and its length overall is $L_{oa} = 82.45$ [m]. Notice that, given the bounds $V_{\max} = 1$ [m/s], $\kappa_v^{\max} = 0.036$ [m/s^2] and $\kappa_v'^{\max} = 0.02$ [m/s^2], the desired relative velocity $U_{rd} = 6$ [m/s] satisfies Assumption 11. The values for the guidance law

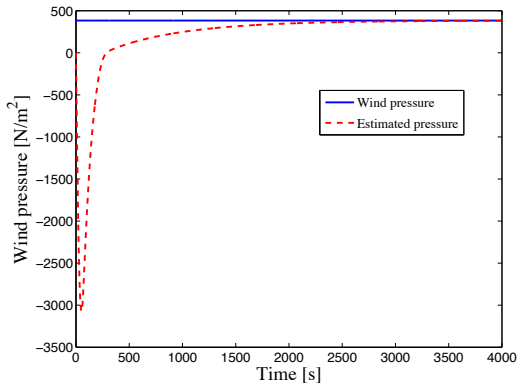

Fig. 6. Adaptive surge-yaw controller estimate $\hat{P}_e(t)$ from simulations. In this case $V_x = -0.41$ [m/s], $V_y = -0.80$ [m/s], $P_e = 382.76$ [N/m^2] and $\beta_e = 286.3$ [deg]. The steady state attack angle is $\gamma_e^{\text{eq}} \approx -96.2$ [deg].

integral gain and look-ahead distance are chosen to satisfy (16-17) and are $\sigma = 1$ [m/s] and $\Delta = 340$ [m]. The adaptive controller (15) is implemented with the following gains: $k_{u_r} = 0.1$, $k_\psi = 0.04$, $k_r = 0.9$ and $\lambda = 0.05$. The adaptation gains are set to $\gamma_1 = 10^6$ and $\gamma_2 = 10^3$. Such high values for γ_1 and γ_2 are necessary to guarantee fast convergence since the quantities $1/m_{11}$ and $1/(m_{22}m_{33} - m_{23}^2)$ render $\kappa_u(\gamma_e)^*$ and $\kappa_r(\gamma_e)^*$ very small (see Appendix I). Finally, the supply vessel has 1600 [kN] of maximum available thrust in surge, while the maximum rudder angle is 35 [deg] and the maximum turning rate is 10 [deg/s]. The ship is given an initial cross track error of 1500 [m] and initially holds zero relative velocity. Its surge axis is parallel to the desired path. Figures 2, 4 and 5 show how the underactuated vessel successfully follows the path $\mathcal{P}$ with a constant side-slip angle $\psi_{ss} \approx -8.0^\circ$ to compensate for the disturbances. Hence, choosing the guidance law parameters according to the criteria (16-17) gives smooth convergence. The relative surge velocity is shown in Figure 5 while the rudder angle is given in Figure 4. Furthermore, Figure 3 shows the performance of the adaption law (15c). As expected, the estimate $\hat{P}_e$ converges to the real value. Notice that for angles of attack that at equilibrium are close to $\gamma_e^{\text{eq}} \approx \pm\pi/2$ convergence is slower as shown in Figure 6. When $\gamma_e \approx \pm\pi/2$ the product $\boldsymbol{G}(\gamma_e)^T\boldsymbol{G}(\gamma_e) > 0$ is at its minimum and therefore the convergence of the persistently exciting (PE) regressor $\boldsymbol{G}(\gamma_e)$ is slower.

IX. Conclusions

Theoretical results and simulations show that the ILOS guidance law from [9], [10] for path following purposes of underactuated surface vessels effectively compensates for kinematic and dynamic disturbances. The ILOS guidance guarantees path following with global κ-exponential stability properties in closed-loop configuration with an adaptive surge-yaw controller, in presence of both the disturbances. A 3DOF control plant model for maneuvering purposes has been introduced where the disturbances are modeled as a combination of a constant irrotational ocean current and constant heading dependent wind forces. Future developments

include improvement of the proposed control plant model and field validation of the proposed guidance law.

APPENDIX I
FUNCTIONAL EXPRESSIONS

$$\kappa_u(\gamma_e)^* = -\frac{1}{m_{11}} A_{Fw} C_X^*(\gamma_e), \tag{33}$$

$$\kappa_r(\gamma_e)^* = -\frac{m_{23} A_{Lw} C_Y^*(\gamma_e)}{m_{22}m_{33} - m_{23}^2} + \frac{m_{22} L_{oa} A_{Lw} C_N^*(\gamma_e)}{m_{22}m_{33} - m_{23}^2}, \tag{34}$$

$$F_{u_r}(u_r, v_r, r) \triangleq \frac{1}{m_{11}}(m_{22}v_r + m_{23}r)r - \frac{d_{11}}{m_{11}}u_r, \tag{35}$$

$$X(u_r) \triangleq \frac{m_{23}^2 - m_{11}m_{33}}{m_{22}m_{33} - m_{23}^2}u_r + \frac{d_{33}m_{23} - d_{23}m_{33}}{m_{22}m_{33} - m_{23}^2}, \tag{36}$$

$$Y(u_r) \triangleq \frac{(m_{22} - m_{11})m_{23}}{m_{22}m_{33} - m_{23}^2}u_r - \frac{d_{22}m_{33} - d_{32}m_{23}}{m_{22}m_{33} - m_{23}^2}, \tag{37}$$

$$\begin{aligned} F_r(u_r, v_r, r) &\triangleq \frac{m_{23}d_{22} - m_{22}(d_{32} + (m_{22} - m_{11})u_r)}{m_{22}m_{33} - m_{23}^2}v_r \\ &+ \frac{m_{23}(d_{23} + m_{11}u_r) - m_{22}(d_{33} + m_{23}u_r)}{m_{22}m_{33} - m_{23}^2}r. \end{aligned} \tag{38}$$

The vectors $\boldsymbol{h}_y \triangleq [h_{y1}, h_{y2}, h_{y3}]^T$, $\boldsymbol{h}_{v_r} \triangleq [h_{v_r1}, h_{v_r2}, h_{v_r3}]^T$ are:

$$\begin{aligned} h_{y1} &= \sin(\tilde{\psi} + \psi_d), \quad h_{y3} = 0, \\ h_{y2} &= U_{rd}\left[\frac{\sin(\tilde{\psi})}{\tilde{\psi}}\cos(\psi_d) + \frac{\cos(\tilde{\psi}) - 1}{\tilde{\psi}}\sin(\psi_d)\right] \\ &+ v_r\left[\frac{\cos(\tilde{\psi}) - 1}{\tilde{\psi}}\cos(\psi_d) - \frac{\sin(\tilde{\psi})}{\tilde{\psi}}\sin(\psi_d)\right], \end{aligned} \tag{39}$$

$$\begin{aligned} h_{v_r1} &= \frac{X(\tilde{u}_r + U_{rd}) - X^{U_rd}}{\tilde{u}_r}\rho(y_{\text{int}}, y, v_r) + \\ &+ v_r\frac{Y(\tilde{u}_r + U_{rd}) - Y^{U_rd}}{\tilde{u}_r}, \\ h_{v_r2} &= \kappa_v(\gamma_e)\Big[\frac{\cos(\tilde{\psi}) - 1}{\tilde{\psi}}\sin(\beta_e - \psi_d) \\ &- \frac{\sin(\tilde{\psi})}{\tilde{\psi}}\cos(\beta_e - \psi_d)\Big], \quad h_{v_r3} = X(\tilde{u}_r + U_{rd}), \end{aligned} \tag{40}$$

where the limits of h_{y2} for $\tilde{\psi} \to 0$ and h_{v_r1} for $\tilde{u}_r \to 0$ exist and are finite. The expression $\rho(y_{\text{int}}, y, v_r)$ is defined as:

$$\begin{aligned} \rho(y_{\text{int}}, y, v_r) &\triangleq \frac{\Delta U_{rd}(y + \sigma y_{\text{int}}) - \Delta^2 v_r}{((y + \sigma y_{\text{int}})^2 + \Delta^2)^{3/2}} \\ &- \frac{\sigma\Delta^2}{((y + \sigma y_{\text{int}})^2 + \Delta^2)^2}y - \frac{\Delta V_y}{(y + \sigma y_{\text{int}})^2 + \Delta^2}. \end{aligned} \tag{41}$$

The wind coefficients from [15] can be smoothed with the following differentiable triangular and square odd wave functions:

$$\text{trg}_{\pi,\text{smooth}} \triangleq \cos^{-1}\Big((1 - \eta)\cos(\gamma_e)\Big) - \frac{\pi}{2}, \tag{42}$$

$$\text{sqr}_{\text{smooth}} \triangleq \frac{1}{\pi}\tan^{-1}\left(\frac{\cos(\gamma_e)}{\eta}\right), \tag{43}$$

where η is an approximation parameter and can be set for instance to 0.01.

REFERENCES

[1] A. J. Sørensen, "Structural issues in the design and operation of marine control systems," *Annual Reviews in Control*, vol. 29, no. 1, pp. 125–149, 2005.

[2] P. Encarnação, A. M. Pascoal, and M. Arcak, "Path following for marine vehicles in the presence of unknown currents," in *Proc. of the 6th IFAC International Symposium on Robot Control*, 2000, pp. 469–474.

[3] I. Kaminer, A. M. Pascoal, and O. Yakimenko, "Nonlinear path following control of fully actuated marine vehicles with parameter uncertainty," in *Proc. of the 16th IFAC World Congress*, 2005.

[4] A. P. Aguiar and J. P. Hespanha, "Trajectory-tracking and path-following of underactuated autonomous vehicles with parametric modeling uncertainty," *IEEE Transactions on Automatic Control*, vol. 52, no. 8, pp. 1362–1379, 2007.

[5] M. Bibuli, M. Caccia, L. Lapierre, and G. Bruzzone, "Guidance of unmanned surface vehicles: Experiments in vehicle following," *IEEE Robotics & Automation Magazine*, vol. 19, no. 3, pp. 92–102, 2012.

[6] G. Indiveri, S. Creti, and A. A. Zizzari, "A proof of concept for the guidance of 3D underactuated vehicles subject to constant unknow disturbances," in *Proc. of the 9th IFAC Conference on Manoeuvring and Control of Marine Craft*, 2012, pp. 307–312.

[7] Y.-S. Kim, H. Lee, and J. Kim, "Coordinated weathervaning control of two surface vessels in a tandem configuration," *Ocean Engineering*, vol. 130, pp. 142–155, 2017.

[8] A. Sans-Muntadas, E. Kelasidi, K. Y. Pettersen, and E. Brekke, "Spiral path planning for docking of underactuated vehicles with limited fov," in *Proc. of IEEE Conference on Control Technology and Applications*, Aug 2017, pp. 732–739.

[9] E. Børhaug, A. Pavlov, and K. Y. Pettersen, "Integral LOS control for path following of underactuated marine surface vessels in the presence of constant ocean currents," in *Proc. of the 47th IEEE Conference on Decision and Control*, 2008, pp. 4984–4991.

[10] W. Caharija, K. Y. Pettersen, M. Bibuli, P. Calado, E. Zereik, J. Braga, J. T. Gravdahl, A. J. Sørensen, M. Milovanović, and G. Bruzzone, "Integral line-of-sight guidance and control of underactuated marine vehicles: Theory, simulations, and experiments," *IEEE Transactions on Control Systems Technology*, vol. 24, no. 5, pp. 1623–1642, Sept 2016.

[11] L. Liu, D. Wang, Z. Peng, and H. Wang, "Predictor-based LOS guidance law for path following of underactuated marine surface vehicles with sideslip compensation," *Ocean Engineering*, vol. 124, pp. 340–348, 2016.

[12] E. Kelasidi, P. Liljebäck, K. Y. Pettersen, and J. T. Gravdahl, "Integral line-of-sight guidance for path following control of underwater snake robots: Theory and experiments," *IEEE Transactions on Robotics*, vol. 33, no. 3, pp. 610–628, June 2017.

[13] T. I. Fossen and A. M. Lekkas, "Direct and indirect adaptive integral line-of-sight path-following controllers for marine craft exposed to ocean currents," *International Journal of Adaptive Control and Signal Processing*, vol. 31, pp. 445–463, 2017.

[14] W. Caharija, K. Y. Pettersen, and J. T. Gravdahl, "Path following of underactuated surface vessels in presence of uknown constant environmental forces: Preliminary results," in *Proc. of the 9th IFAC Conference on Control Applications in Marine Systems*, 2013, pp. 85–90.

[15] W. Blendermann, "Parameter identification of wind loads on ships," *Journal of Wind Engineering and Industrial Aerodynamics*, vol. 51, no. 3, pp. 339–351, 1994.

[16] T. I. Fossen, *Handbook of Marine Craft Hydrodynamics and Motion Control*. Hoboken, NJ: John Wiley & Sons, Inc., 2011.

[17] O. M. Faltinsen, *Sea Loads on Ships and Offshore Structures*. Cambridge University Press, 1990.

[18] T. I. Fossen, A. Loría, and A. R. Teel, "A theorem for UGAS and ULES of (passive) nonautonomous systems: robust control of mechanical systems and ships," *International Journal of Robust and Nonlinear Control*, vol. 11, no. 2, pp. 95–108, 2001.

[19] S. Fan and C. A. Woolsey, "Underwater vehicle control and estimation in nonuniform currents," in *Proc. of American Control Conference*, 2013, pp. 1400–1405.

[20] K. Reichert, K. Hessner, J. C. N. Borge, and J. Dittmer, "WaMoS II: A radar based wave and current monitoring system," in *Proc. of International Offshore and Polar Engineering Conference*, 1999, pp. 139–143.

[21] R. M. Isherwood, "Wind resistance of merchant ships," *Transcripts of the Royal Institution of Naval Architects*, vol. 115, pp. 327–338, 1972.

[22] OCIMF, *Prediction of Wind and Current Loads on VLCCs*. London, UK: Oil Companies International Marine Forum, 1977.

[23] E. Panteley and A. Loría, "On global uniform asymptotic stability of nonlinear time-varying systems in cascade," *Systems and Control Letters*, vol. 33, no. 2, pp. 131–138, 1998.

[24] E. Panteley, E. Lefeber, A. Loría, and H. Nijmeijer, "Exponential tracking control of a mobile car using a cascaded approach," in *Proc. of IFAC Workshop on Motion Control*, 1998, pp. 221–226.

[25] E. Fredriksen and K. Y. Pettersen, "Global κ-exponential way-point manoeuvering of ships," in *Proc. of the 43rd IEEE Conference on Decision and Control*, 2004, pp. 5360–5367.